materials

MDPI

Article

$SnAg_2O_3$-Coated Adhesive Tape as a Recyclable Catalyst for Efficient Reduction of Methyl Orange

Kalsoom Akhtar *, Asma A. Alhaj, Esraa M. Bakhsh, Sher Bahadar Khan and Taghreed M. Fagieh

Chemistry Department, Faculty of Science, King Abdulaziz University, P.O. Box 80203, Jeddah 21589, Saudi Arabia; aalhaj0007@stu.kau.edu.sa (A.A.A.); ibakhsh@kau.edu.sa (E.M.B.); sbhkhan@kau.edu.sa (S.B.K.); tfagieh@kau.edu.sa (T.M.F.)

* Correspondence: kaskhan@kau.edu.sa

Abstract: Silver oxide-doped tin oxide ($SnAg_2O_3$) nanoparticles were synthesized and different spectroscopic techniques were used to structurally identify $SnAg_2O_3$ nanoparticles. The reduction of 4-nitrophenol (4-NP), congo red (CR), methylene blue (MB), and methyl orange (MO) was studied using $SnAg_2O_3$ as a catalyst. Only 1.0 min was required to reduce 95% MO; thus, $SnAg_2O_3$ was found to be effective with a rate constant of 3.0412 min^{-1}. Being a powder, $SnAg_2O_3$ is difficult to recover and recycle multiple times. For this reason, $SnAg_2O_3$ was coated on adhesive tape (AT) to make it recyclable for large-scale usage. $SnAg_2O_3$@AT catalyst was assessed toward MO reduction under various conditions. The amount of $SnAg_2O_3$@AT, $NaBH_4$, and MO was optimized for best possible reduction conditions. The catalyst had a positive effect since it speed up the reduction of MO by adding more $SnAg_2O_3$@AT and $NaBH_4$ as well as lowering the MO concentration. $SnAg_2O_3$@AT totally reduced MO (98%) in 3.0 min with a rate constant of 1.3669 min^{-1}. These findings confirmed that $SnAg_2O_3$@AT is an effective and useful catalyst for MO reduction that can even be utilized on a large scale for industrial purposes.

Keywords: $SnAg_2O_3$; $SnAg_2O_3$@AT; nanocatalyst; pollutants; methyl orange; reduction

check for updates

Citation: Akhtar, K.; Alhaj, A.A.; Bakhsh, E.M.; Khan, S.B.; Fagieh, T.M. $SnAg_2O_3$-Coated Adhesive Tape as a Recyclable Catalyst for Efficient Reduction of Methyl Orange. *Materials* **2023**, *16*, 6978. https://doi.org/10.3390/ma16216978

Academic Editor: Barbara Pawelec

Received: 22 August 2023
Revised: 16 October 2023
Accepted: 17 October 2023
Published: 31 October 2023

Copyright: © 2023 by the authors. Licensee MDPI, Basel, Switzerland. This article is an open access article distributed under the terms and conditions of the Creative Commons Attribution (CC BY) license (https://creativecommons.org/licenses/by/4.0/).

1. Introduction

Recently, much attention has been given to heterogeneous catalysis because of the enormously important role it plays in environmentally and industrially significant catalytic reactions. Catalysis has extensive applications, comprising the synthesis of crucial pharmaceutical scaffolds, the transformation of harmful chemicals into useful ones, the degradation and reduction of contaminants and toxins, etc. However, the effectiveness and durability of catalysts play a major part in catalysis [1–3]. Therefore, the primary goal of catalysis is to prepare stable and effective catalysts, which have high catalytic activities on a large scale. The catalyst's ability to catalyze reactions is mostly determined by the catalyst's active sites, the molecules' ability to interact with the catalyst, and the mass transformation of the reacting molecules into the product [4–6]. Therefore, it is essential to design effective catalysts with extraordinary efficiency for industrial and environmental purposes [7–9].

The most effective catalysts are metal oxides, which are frequently utilized in numerous industrial and environmental applications [10–15]. Tin oxide (SnO_2) nanomaterials have attracted a lot of attention and have proven their efficiency as crucial heterogeneous catalysts. SnO_2 is an effective catalyst that has been used in a variety of environmental applications and synthetic reactions. SnO_2 has been employed in photo-catalysis, catalysis, Li-ion batteries, sensing, and other processes [16–18]. However, doped metal oxides and metal oxide nanocomposites are substantially more effective, stable, and competent catalysts for several processes, therefore, it has gained considerable attention. Metal oxides can be doped with other metals to increase their surface area and reaction sites, which improves the catalyst's ability to catalyze various reactions. Because doping affects the

characteristics of metal oxides and demonstrated outstanding catalytic activity in several catalytic reactions [19–22]. Thus, in response to the growing demand for synthetic and environmental applications, silver oxide-tin oxide nanocomposite was prepared to improve catalytic efficiency. However, $SnAg_2O_3$ is a powder, thus, one of the main issues with powder catalysts is that they tend to aggregate, which limits its ability to catalyze. The powder catalyst also cannot be recycled and used again by merely recovering it from the reaction medium. Therefore, to make the catalyst easier to reuse, polymeric or other supports can be employed since they play a significant role as hosts for metal oxides and other nanomaterials [23–26]. Benali et al. developed a catalyst based on a Zn(II)-crosslinked alginate loaded with Ag NPs for dye reduction [27]. Mallakpour et al. reported the catalytic reduction of nitrophenols, dyes, and metal ion pollutants based on mesoporous Ca-alginate/melamine-rich covalent organic polymer/cupric oxide microgel beads [28]. Meena and Saini described the synthesis of a PANI/ZnO/MnO_2 ternary nanocomposite which was employed in the catalytic reduction of 4-nitrophenol as well as the adsorption of crystal violet dye from aqueous solutions [29].

Here, $SnAg_2O_3$ nanoparticles were synthesized and structurally characterized via numerous techniques. After that, the catalytic performance of $SnAg_2O_3$ was evaluated for the catalytic reduction of several contaminants. To examine the catalytic ability of $SnAg_2O_3$, the catalytic reduction of dyes and nitrophenols was used as a model electron exchange process. $SnAg_2O_3$ was discovered to be an effective catalyst and subsequently used for catalytic reactions involving electron transfers in 4-NP, MO, CR, and MB reduction. $SnAg_2O_3$ was found to be effective for MO reduction and it was revealed that the catalyst amount has a beneficial impact and greatly improves the reaction rate. Further, $SnAg_2O_3$ was coated on AT to make the catalyst easier to be recycled. In the reduction of MO, BH_4^- ions diffuse into the surface of $SnAg_2O_3$ and $SnAg_2O_3$@AT in the first stage, where borohydride injects electrons onto the catalyst. Then, the electrons are subsequently transferred to MO. These catalysts serve as an electron relay. Thus, $SnAg_2O_3$ and $SnAg_2O_3$@AT are excellent nanocatalysts for the reduction of MO. The prepared nanocatalysts have the potential to compete and eventually substitute the well-known commercial catalysts because of their superior efficiency, cost-effectiveness, and simplicity in processing. The novelty of the developed efficient catalyst is that it overcomed the limitations like aggregation, regeneration, and non-recyclability. These limitations could be avoided by coating $SnAg_2O_3$ on AT support which made the reuse of the $SnAg_2O_3$ catalyst easier. AT was used as a support on which $SnAg_2O_3$ was coated by just rubbing where the glue had bound the catalyst. The coating of a powder catalyst is an ideal method for the advancement of the catalyst because it is a challenge to implement powder nanomaterials as a catalyst for large scale application. The coating of powder nanomaterials on a flexible support was developed to address the problems of aggregation and recyclability. This allowed powder catalysts to be recyclable and widen the catalyst applicability.

2. Experimental

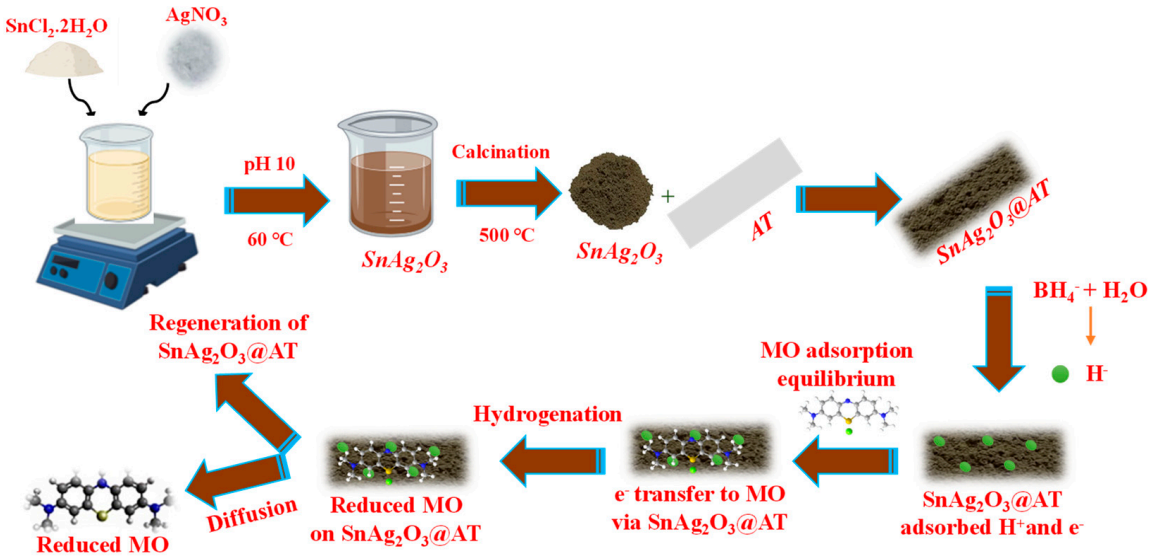
2.1. Reagents and Chemicals

Sodium borohydride ($NaBH_4$, 97%) was purchased from BDH chemicals, England. Silver chloride, tin chloride, 4-nitrophenol (4-NP), congo red (CR), methyl orange (MO), and methylene blue (MB) were purchased from Sigma-Aldrich. To prepare all solutions, distilled water was utilized. Adhesive tape, which is normally used for packing purposes, was bought from the local market and used as a supporting glue-based tape for the catalyst.

2.2. Preparation of $SnAg_2O_3$ and $SnAg_2O_3$@AT

Initially, the solution was made by placing the salts of $AgNO_3$ and $SnCl_2.2H_2O$ in 100 mL of water, and stirring the mixture (1:1 molar ratio) for 30 min. Then, the pH of the solution was adjusted to 10 by dropping NaOH solution, and the solution was stirred continuously at 60.0 °C overnight while being kept on a hot plate stirrer [17,18]. As soon as the reaction was stopped, $SnAg_2O_3$ settled down as a precipitate. Then, $SnAg_2O_3$

was washed, dried, and then further calcined for five hours at 500 °C. $SnAg_2O_3$@AT was prepared by coating $SnAg_2O_3$ on AT, as shown in Scheme 1.



Scheme 1. Graphic illustration of $SnAg_2O_3$@AT nanocatalyst preparation and its application in MO reduction.

2.3. Characterization of $SnAg_2O_3$

The morphology of $SnAg_2O_3$ was examined using a JEOL Scanning Electron Microscope (JSM-7600F, Akishima-shi, Japan). $SnAg_2O_3$ elemental composition was determined using the Oxford-EDS technique for Energy-Dispersive X-Ray Spectrometry (EDS). Thermo Scientific's (Waltham, MA, USA) X-ray diffractometer was used to study the crystal structure of $SnAg_2O_3$. Thermo Fisher Scientific's NicoletTM iS50 FTIR Spectrometer was used to identify the functional groups of $SnAg_2O_3$. Using a Thermo Scientific Evolution 300 UV-vis spectrometer, spectral data for all chemicals were recorded over the wavelength range of 200–800 nm.

2.4. Catalytic Studies of $SnAg_2O_3$ and $SnAg_2O_3$@AT

$SnAg_2O_3$ was initially used for the selectivity study of a reduction reaction of 4-NP, CR, MB, and MO. Each compound's reduction was evaluated after 2.5 mL of 4-NP (0.1 mM), CR (0.07 mM), MB (0.07 mM), and MO (0.07 mM) were individually mixed with 0.5 mL of $NaBH_4$ (0.1 M) and verified each compound's decrease. The reduction was then observed by continuously measuring the UV-vis spectra of CR, MB, and MO at maximum wavelengths of 488 nm, 660 nm, and 460 nm, respectively. However, after adding $NaBH_4$, 4-NP was tested at 400 nm due to the production of nitrophenolate ions. Next, $SnAg_2O_3$ (20 mg) was added to each compound. Because $SnAg_2O_3$ was found to be more efficient and selective for MO reduction, $SnAg_2O_3$@AT was evaluated for further reduction studies using 0.02 mM, 0.05 mM, and 0.07 mM of MO, with 0.3 mL, 0.5 mL, and 1.0 mL of $NaBH_4$, using 5.5, 8.5 and 9.5 mg of $SnAg_2O_3$@AT, and different reduction parameters were optimized.

The following Equation (1) was used to estimate the percent reduction of each pollutant [30–32]:

$$\%Reduction = \frac{C_o - C_t}{C_o} \times 100 = \frac{A_o - A_t}{A_o} \times 100 \quad (1)$$

where $C_o = A_o$ = initial concentration and $C_t = A_t$ = final concentration of each compound.

3. Results and Discussion

3.1. Catalyst Selection

The efficiency, stability, and reusability of the catalyst are three crucial considerations that should be taken into account in preparing an effective catalyst. Several catalysts are effective; however, they have issues with stability and reusability. In order to minimize the recyclability difficulties and provide a reliable catalyst for industrial and commercial large-scale use, an effective catalyst was prepared based on $SnAg_2O_3$ and further used to coat an AT. $SnAg_2O_3$ was made as a powder, however, powder catalysts typically suffer from aggregation, separation, and recyclability issues. Several spectroscopy approaches were used to structurally study the prepared $SnAg_2O_3$ and $SnAg_2O_3$@AT.

3.2. Physiochemical Characterization of $SnAg_2O_3$

SEM images of the $SnAg_2O_3$ nanocatalyst, shown in Figure 1, were used to determine its size and surface morphology. According to the SEM pictures at various magnifications, $SnAg_2O_3$ had a morphology like well-scattered particles. The particles were found to have grown in significant numbers while maintaining their spherical form.

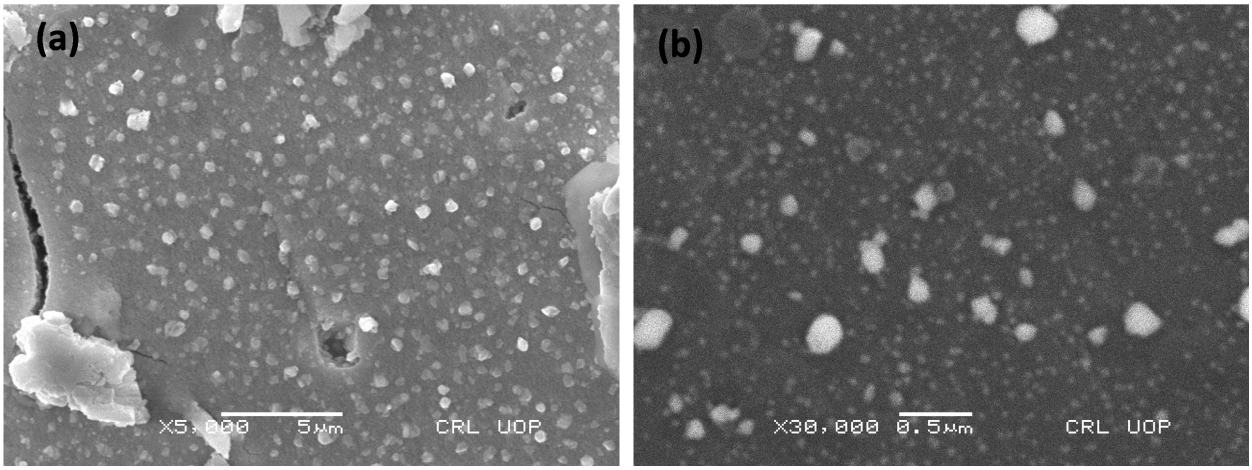
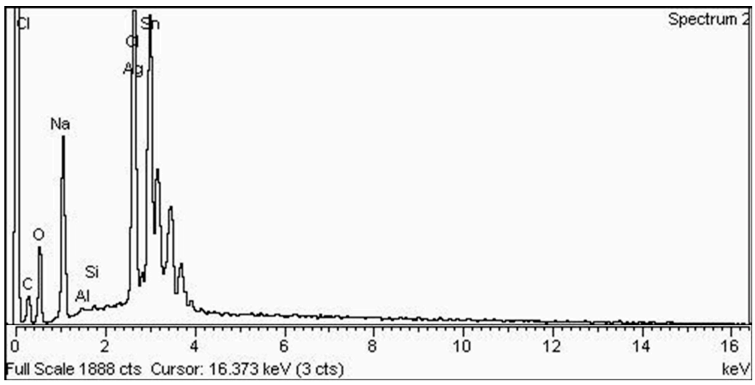


Figure 1. SEM images of the $SnAg_2O_3$ nanocatalyst at (**a**) low and (**b**) high magnifications.

The elemental composition of $SnAg_2O_3$ was verified via EDS. According to the EDS analysis, Sn, Ag, and O peaks were observed at around 1.5, 2.6 and 3.0 kV with respective weight percentages of 14.51%, 32.79%, and 20.27%, respectively, as shown in Figure 2. The spectrum showed that $SnAg_2O_3$ comprised Sn, Ag, and O, in which Ag had the highest mass percentage, indicating that it was the primary component of $SnAg_2O_3$. The EDS spectrum indicated that the preparation of $SnAg_2O_3$ was successful.

X-ray diffraction confirmed the crystal structure for $SnAg_2O_3$ (Figure 3a). The $SnAg_2O_3$ XRD pattern showed many intense peaks at 26.6°, 27.8°, 32.2°, 33.5°, 38.0°, 46.1°, 52.2°, 54.7°, 57.4°, and 64.4°. The typical diffraction peaks of low intensities at 26.6°, 33.5°, 52.2°, and 64.4°, which were indexed to (110), (101), (211), and (301) planes fitting with tetragonal SnO_2. The characteristic hexagonal Ag_2O peaks of (110), (111), (200), (211), (220), and (221) planes were shown at 27.8°, 32.2°, 38.0°, 46.1°, 54.4°, and 57.4°, respectively. The XRD pattern perfectly matched the hexagonal Ag_2O and tetragonal SnO_2 crystal structures [33,34]. This indicated that the material includes both Ag_2O and SnO_2 according to the XRD spectrum of $SnAg_2O_3$.



Element	Weight%	Atomic%
C K	8.01	20.58
O K	20.27	39.11
Na K	12.33	16.55
Al K	0.15	0.17
Si K	0.17	0.19
Cl K	11.77	10.25
Ag L	32.79	9.38
Sn L	14.51	3.77
Totals	100.00	

Figure 2. EDS spectrum and weight percent of $SnAg_2O_3$ nanocatalyst.

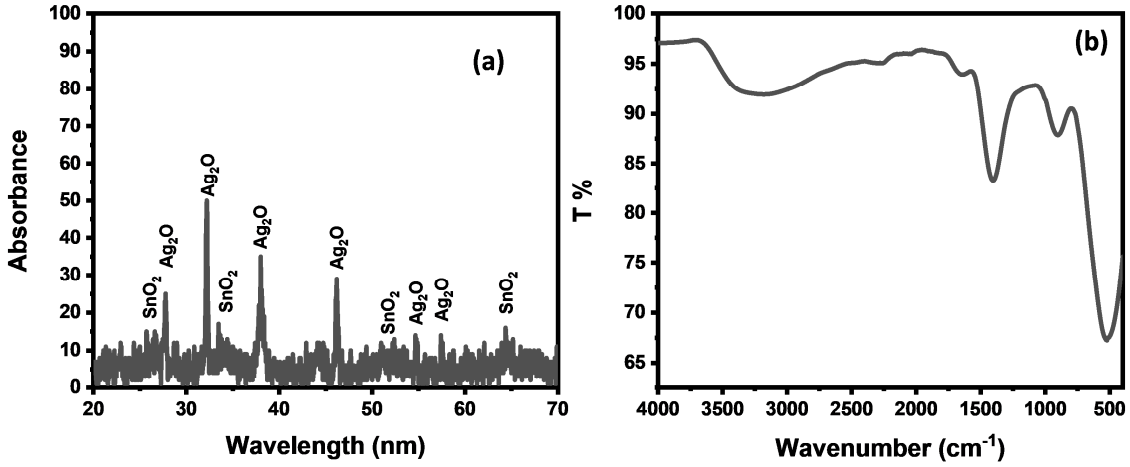


Figure 3. (**a**) XRD and (**b**) ATR-FTIR of $SnAg_2O_3$ nanocatalyst.

ATR-FTIR analysis was used to evaluate the $SnAg_2O_3$ nanocatalyst chemical composition. The $SnAg_2O_3$ ATR-FTIR spectrum showed a strong band at 519 cm^{-1} (Figure 3b) that was responsible for the M–O bond (M = Sn, Ag). Additionally, the OH group broad bands were observed at 3200 cm^{-1} and 1637 cm^{-1}. It also showed two bands at 901 cm^{-1} and 1404 cm^{-1}, which were responsible for the nitrate group, suggesting that $SnAg_2O_3$ may contain the nitrate of the precursor. The FTIR spectrum of the prepared nanocatalyst supports the growth of $SnAg_2O_3$.

4. Catalytic Properties of $SnAg_2O_3$

In order to assess the $SnAg_2O_3$ catalytic impact, it was first evaluated as a nanocatalyst for the reduction of 4-NP, CR, MB, and MO via a reducing agent. Initially, only a modest amount (20 mg) of $SnAg_2O_3$ was scrutinized in the reduction process of each individual pollutant. Figure 4 clearly shows that the absorbance of 4-NP, CR, MB, and MO gradually decreased, indicating that $SnAg_2O_3$ had a positive impact on their reduction. These findings confirm that the $SnAg_2O_3$ nanocatalyst reduced MO and CR within 1.0 min and 8.0 min, respectively, while it took 4.0 min to reduce both MB and 4-NP. Using Equation (1), the percentage reduction was further computed, and it was found that the $SnAg_2O_3$ nanocatalyst reduced 95.77% of 4-NP, 93.12% of CR, 95.23% of MB, and 95.22% of MO (Figure 5a).

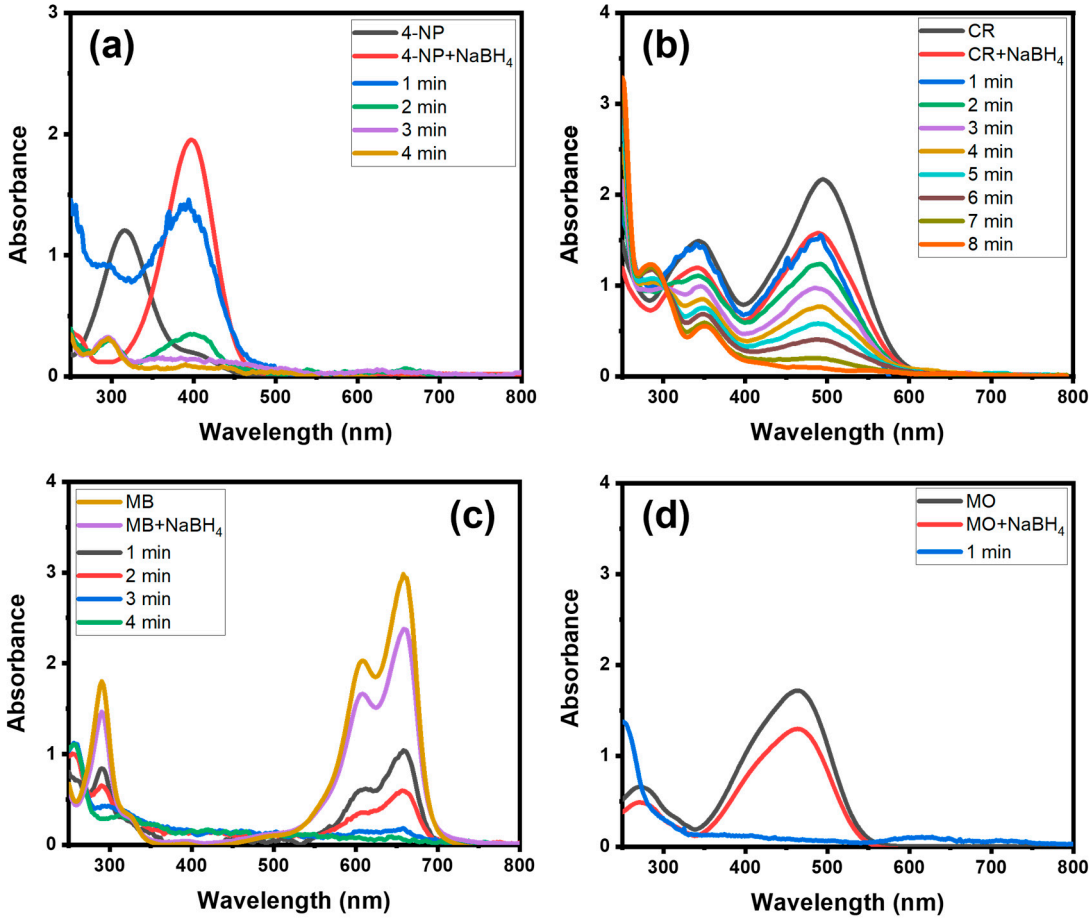


Figure 4. Time-dependent UV–vis spectra of (**a**) 4-NP, (**b**) CR, (**c**) MB, and (**d**) MO using 20 mg of $SnAg_2O_3$ and 0.5 mL of $NaBH_4$.

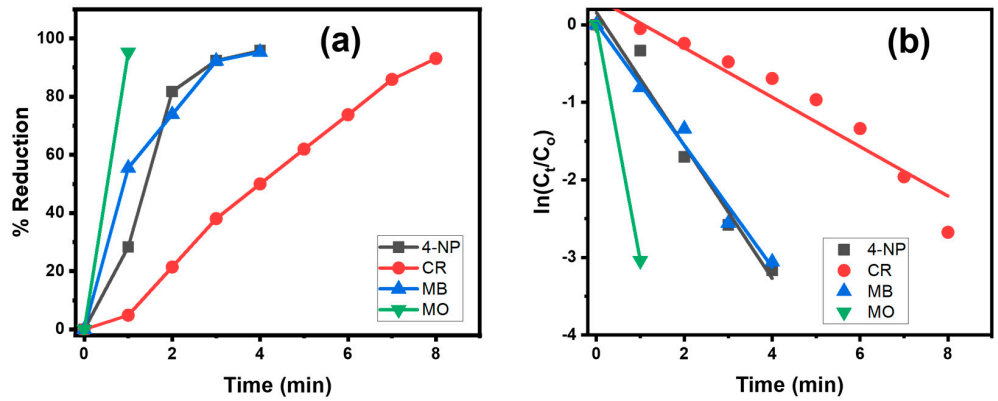


Figure 5. (**a**) % Reduction and (**b**) kinetics using 20 mg of $SnAg_2O_3$ and 0.5 mL of $NaBH_4$ for reduction of different pollutants.

Further, to examine the rate constants for all pollutants that are reduced in the presence of $SnAg_2O_3$, the pseudo-first-order kinetic presented in Equation (2) was used [35–37]:

$$\ln C_t/C_o = \ln A_t/A_o = -K_t \quad (2)$$

where $A_t = C_t$ is the absorbance or concentration of reduced pollutant at various reaction times, $A_o = C_o$ is the absorbance or reducing chemical concentration prior to the reaction,

and K (min^{-1}) is the slope-based rate constant calculated from the graph of ln C_t/C_o vs. $SnAg_2O_3$ reduction time (Figure 5b).

The rate constant values for 4-NP, CR, MB, and MO reduction reactions using $SnAg_2O_3$ were 0.8573 min^{-1}, 0.3186 min^{-1}, 0.7859 min^{-1}, and 3.0412 min^{-1}, respectively. This suggested that $SnAg_2O_3$ is selective for MO reduction. Therefore, $SnAg_2O_3$ was more efficient in reducing MO based on the rate constants that reflect its catalytic activity.

Since MO reduction was completed using $SnAg_2O_3$ in 1.0 min, it was selected for the comprehensive analysis and optimization of reaction conditions using the $SnAg_2O_3$@AT nanocatalyst. Only $SnAg_2O_3$@AT was used for further MO reduction investigations in order to minimize recycling concerns and provide a superior catalyst for large-scale applications since powder catalysts have problems with aggregation, separation, and recyclability.

4.1. Catalytic Activity of $SnAg_2O_3$@AT toward MO

$SnAg_2O_3$@AT was used for MO reduction to test the catalytic activity. The reduction of 2.5 mL of MO (0.07 mM) was first investigated in the presence of only $NaBH_4$. Without $SnAg_2O_3$ or $SnAg_2O_3$@AT, a negligible reduction took place, and the concentration of MO was slightly changed. This demonstrates unequivocally that a catalyst is necessary for MO reduction. To reduce MO effectively, $SnAg_2O_3$@AT was added and the reaction was monitored by measuring UV-vis absorption. The $NaBH_4$ + MO reaction was initially investigated with 8.5 mg of $SnAg_2O_3$@AT.

Since there was a steady loss of the MO color as the reaction progressed along with the drop in absorbance, the reduction of MO was visually detected. This shift in color and drop in absorbance indicated MO reduction, which occurred in 1.0 min and 3.0 min by employing 20 mg of $SnAg_2O_3$ and 8.5 mg of $SnAg_2O_3$@AT, as shown in Figure 6.

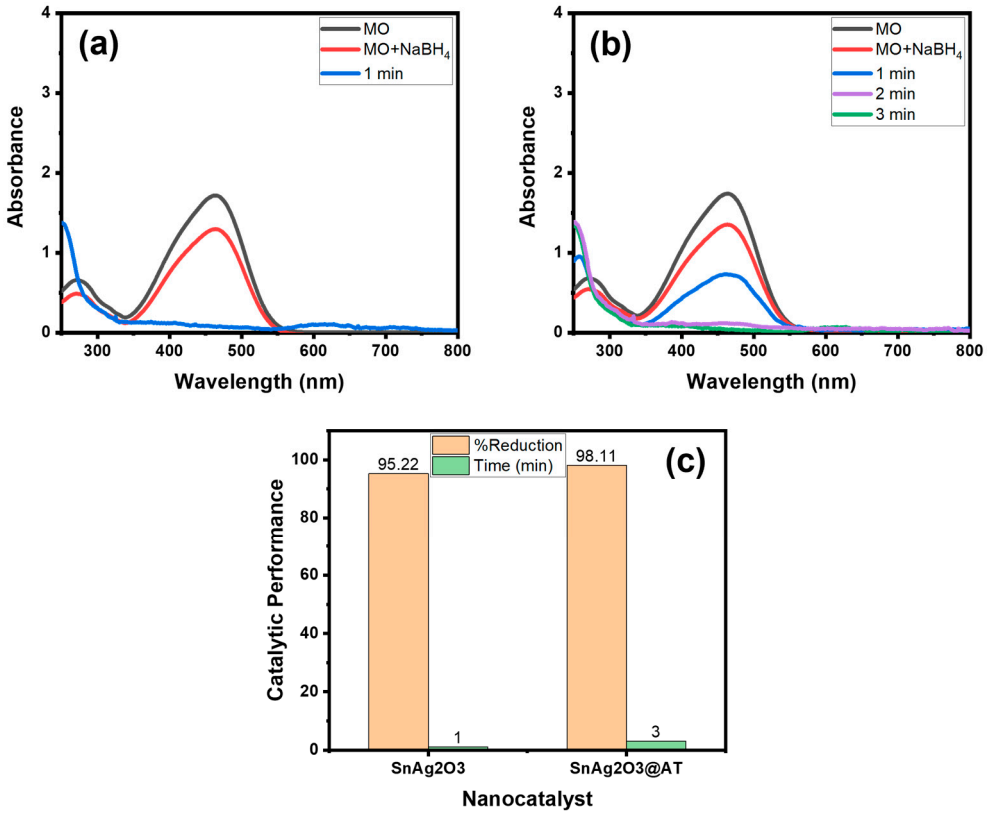


Figure 6. Time-dependent UV–vis spectra for MO reduction using (**a**) 20 mg of $SnAg_2O_3$ and (**b**) 8.5 mg of $SnAg_2O_3$@AT and 0.5 mL of $NaBH_4$. (**c**) Comparison of nanocatalysts' catalytic performance toward MO reduction.

Equation (2) was also used to determine the kinetic reduction of MO via $SnAg_2O_3$@AT. As a result, K was found to be 1.3669 min^{-1} (Figure 7b). As indicated in Table 1, the rate constants of $SnAg_2O_3$ and $SnAg_2O_3$@AT were also compared with those of other reported catalysts.

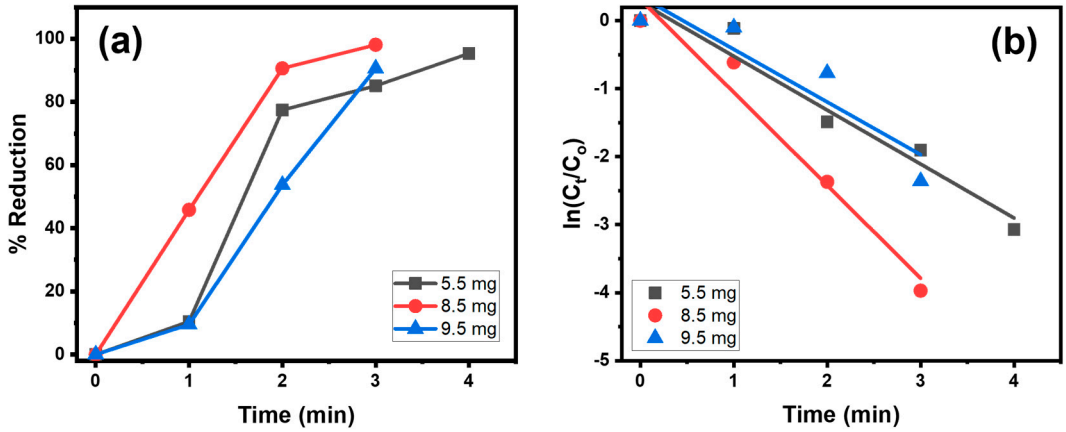


Figure 7. (**a**) % Reduction and (**b**) kinetics of MO reduction by 0.5 mL of $NaBH_4$ using different amounts of $SnAg_2O_3$@AT (5.5 mg, 8.5 mg, and 9.5 mg).

Table 1. Rate constant comparison of $SnAg_2O_3$ and $SnAg_2O_3$@AT with literature.

Catalyst	Rate Constant (min^{-1})	Reference
Alg-tin oxide–cobalt oxide	1.2775	[18]
AuNPs	0.1020	[38]
Pd NPs	0.0909	[39]
K-AgNPs	0.0286	[40]
WBs loaded with Ni NPs	0.1500	[41]
CuSnOS/AC	1.1480	[42]
Cu@Alg/BP	0.2702	[43]
Sd@Ag-NPs	0.3850	[44]
$SnAg_2O_3$	3.0412	This Study
$SnAg_2O_3$@AT	1.3669	This Study

4.1.1. Effect of $SnAg_2O_3$@AT Dosage

To explore the dose effect, 2.5 mL of MO was reduced by 0.5 mL of $NaBH_4$ (0.1 M) in the presence of 5.5 mg, 8.5 mg, and 9.5 mg of $SnAg_2O_3$@AT. With a high dose of $SnAg_2O_3$@AT, the reduction process of MO occurred more rapidly. MO reduction with 8.5 mg and 9.5 mg of $SnAg_2O_3$@AT took only 3.0 min, which was faster than the lower dose (took 4.0 min). Equations (1) and (2) were used to determine the catalytic efficiency of $SnAg_2O_3$@AT in the reduction of MO, as illustrated in Figure 7, which showed that a superior reduction was quickly achieved by utilizing 8.5 mg of $SnAg_2O_3$@AT (98.11%) in just 3.0 min with a rate constant of 1.3669 min^{-1}. By using 9.5 mg, $SnAg_2O_3$@AT reduced 90.56% of MO (K = 0.7751 min^{-1}). On the other hand, 5.5 mg reduced 95.36% of MO in 4.0 min (K = 0.7936 min^{-1}). These findings demonstrated that the amount of the catalyst has a beneficial effect on MO reduction because it is directly related to the percent reduction.

4.1.2. Effect of $NaBH_4$ Concentration

To examine the influence of $NaBH_4$ concentration, 0.3 mL, 0.5 mL, and 1.0 mL of $NaBH_4$ (1.0 M) were studied on the reduction of 2.5 mL of MO utilizing 8.5 mg of $SnAg_2O_3$@AT. The findings showed that $NaBH_4$ had a negligible impact on $SnAg_2O_3$@AT ability to reduce MO. It was discovered that 8.5 mg of $SnAg_2O_3$@AT reduced 94.94% and 98.11% of MO in 5.0 min and 3.0 min, respectively, using 0.3 mL and 0.5 mL of $NaBH_4$.

While applying 1.0 mL of $NaBH_4$, 8.5 mg of $SnAg_2O_3$@AT reduced 85.34% of MO in 1.0 min. As a result, it was discovered that by adding more $NaBH_4$ (0.3 mL~1.0 mL), the MO reduction reaction rate was increased using $SnAg_2O_3$@AT, in which the rate constants were 0.6301 min^{-1}, 1.3669 min^{-1}, and 1.9199 min^{-1} for 0.3 mL, 0.5 mL, and 1.0 mL, respectively, as illustrated in Figure 8. Specifically, $SnAg_2O_3$@AT transfers electrons from BH_4^- to MO. However, if the concentration of electron-rich moieties is in a large quantity, there is still competition for electrons to reach MO, which may reduce the % reduction of MO as a result of competition and steric hindrance. Overall, it can be concluded that the amount of $NaBH_4$ has a good impact on MO reduction when it is used in appropriate amounts.

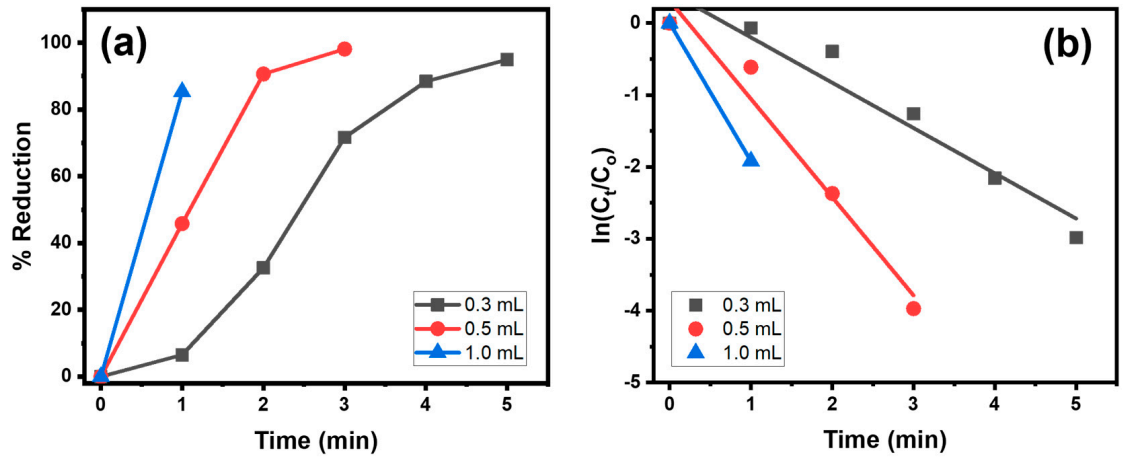


Figure 8. (**a**) % Reduction and (**b**) kinetics of MO reduction using 8.5 mg of $SnAg_2O_3$@AT in the presence of $NaBH_4$ (0.3 mL, 0.5 mL, and 1.0 mL).

4.1.3. Effect of MO Concentration

To assess the catalytic behavior of $SnAg_2O_3$@AT, the reduction process was tested using various concentrations of MO. A total of 8.5 mg of $SnAg_2O_3$@AT was utilized for the reduction of 2.5 mL of MO + 0.5 mL of $NaBH_4$, in which the concentrations of MO were 0.02 mM, 0.05 mM, and 0.07 mM. As illustrated in Figure 9, it was discovered that $SnAg_2O_3$@AT reduced 0.02 mM MO much faster (2.0 min) than 0.05 mM and 0.07 mM (3.0 min). This means that higher concentrations of MO require more time to be reduced than lower concentrations. Accordingly, there is a direct proportion between the concentration of MO and its reduction time.

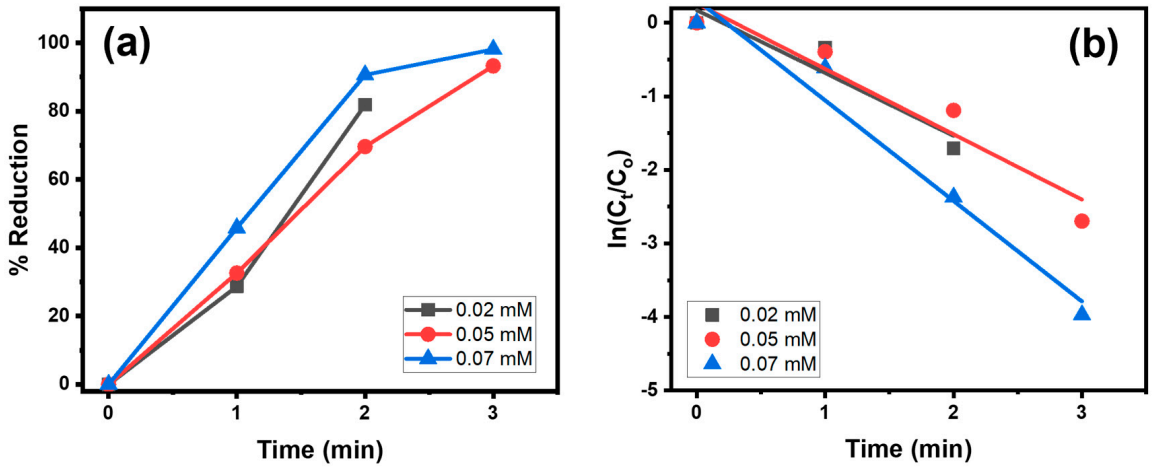


Figure 9. (**a**) % Reduction and (**b**) kinetics of MO reduction (0.02 mM, 0.05 mM, and 0.07 mM) using 8.5 mg of $SnAg_2O_3$@AT and 0.5 mL of $NaBH_4$.

4.1.4. Recyclability

The stability and reusability of a catalyst are important factors from an economic and environmental perspective [45–47]. Thus, $SnAg_2O_3$@AT was investigated for recyclability. The recyclability of $SnAg_2O_3$@AT was evaluated by performing a reduction of 2.5 mL MO (0.07 mM). Three further reactions were analyzed using 8.5 mg of $SnAg_2O_3$@AT. It was simple to remove $SnAg_2O_3$@AT from the reaction medium after each use. Then, $SnAg_2O_3$@AT was cleaned with distilled water before being used in the following process. In the first, second, and third cycles, the data showed that $SnAg_2O_3$@AT completely (>94%) reduced MO in 3.0, 5.0, and 8.0 min, respectively. Figure 10 shows the catalytic activity of $SnAg_2O_3$@AT in each cycle.

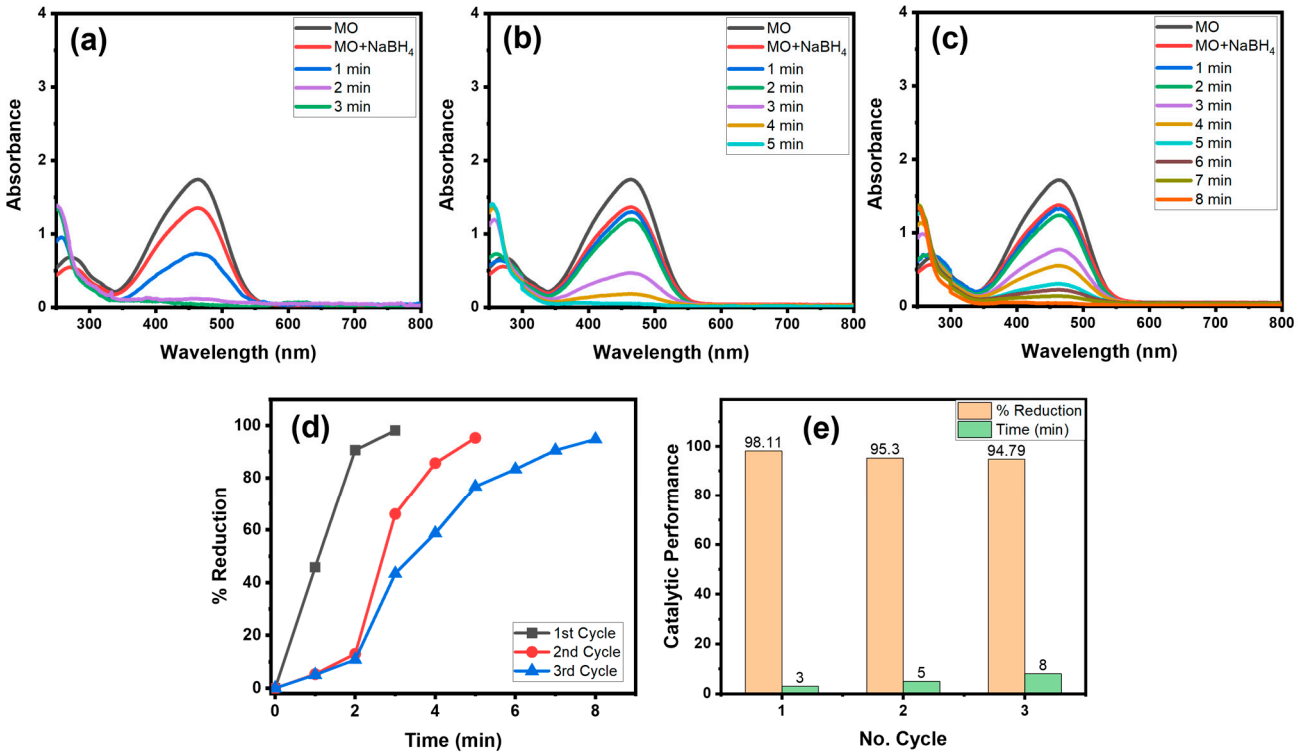


Figure 10. Time-dependent UV–vis spectra for reduction of 0.07 mM MO; (**a**) 1st cycle, (**b**) 2nd cycle, and (**c**) 3rd cycle using 8.5 mg of $SnAg_2O_3$@AT and 0.5 mL of $NaBH_4$. (**d**) % Reduction of MO using 8.5 mg of $SnAg_2O_3$@AT for three cycles. (**e**) Recyclability performance of $SnAg_2O_3$@AT nanocatalyst in MO reduction.

The results showed that $SnAg_2O_3$@AT was able to effectively reduce MO in 8.0 min up to the third cycle, which indicated the stability and recyclability of the material based on the catalytic activity in each cycle. These findings imply that $SnAg_2O_3$@AT can be used repeatedly without significant losing of its superior catalytic activity.

4.1.5. Mechanism of MO Reduction

The process of the catalytic reduction of MO depends on catalyst-mediated electron transmittance. $NaBH_4$ dissociates initially into BH_4^- and gets adsorbed on $SnAg_2O_3$@AT, where it donates electrons to the surface of $SnAg_2O_3$@AT which then attack MO molecules. Azo bonds are activated by electrons existing on the surface of $SnAg_2O_3$@AT when MO molecules get adsorbed onto it. As a result, the breakage of azo bonds takes place, thus, the formation of aromatic amines occurs during the reduction process resulting in the disappearance of MO color which confirms the completion of its catalytic reduction.

5. Conclusions

This study demonstrated the straightforward manufacturing of $SnAg_2O_3$ nanomaterial, which was successfully produced using the co-precipitation method. With the help of SEM, EDS, XRD, and FTIR, the physiochemical characterization of $SnAg_2O_3$ was examined. The reduction of different compounds was investigated (4-NP, CR, MB, and MO) in the presence of $SnAg_2O_3$. Using $SnAg_2O_3$ and $SnAg_2O_3$@AT, MO was reduced within 1.0 min and 3.0 min with $NaBH_4$ at reduction rates of 3.0412 min^{-1} and 1.3669 min^{-1}, respectively. Thus, based on the catalytic activities, $SnAg_2O_3$ and $SnAg_2O_3$@AT were specified as efficient catalysts for the MO reduction. MO reduction was therefore selected for further analysis and reaction condition optimization. The results suggested that $SnAg_2O_3$@AT is a stable and recyclable catalyst for the catalytic reduction of industrial dyes.

Author Contributions: Conceptualization, S.B.K.; Methodology, A.A.A. and S.B.K.; Investigation, E.M.B.; Writing—original draft, K.A.; Writing—review & editing, A.A.A., E.M.B., S.B.K. and T.M.F.; Funding acquisition, K.A. All authors have read and agreed to the published version of the manuscript.

Funding: The Deanship of Scientific Research (DSR) at King Abdulaziz University (KAU), Jeddah, Saudi Arabia has funded this project under grant no. (G: 529-247-1443).

Institutional Review Board Statement: Not applicable.

Informed Consent Statement: Not applicable.

Data Availability Statement: The data presented in this study are available on request from the corresponding author.

Conflicts of Interest: The authors declare no conflict of interest.

References

1. Mabate, T.P.; Maqunga, N.P.; Ntshibongo, S.; Maumela, M.; Bingwa, N. Metal oxides and their roles in heterogeneous catalysis: Special emphasis on synthesis protocols, intrinsic properties, and their influence in transfer hydrogenation reactions. *SN Appl. Sci.* **2023**, *5*, 196.
2. Chen, F.; Jiang, X.; Zhang, L.; Lang, R.; Qiao, B. Single-atom catalysis: Bridging the homo- and heterogeneous catalysis. *Chin. J. Catal.* **2018**, *39*, 893–898. [CrossRef]
3. Guan, Y.; Chaffart, D.; Liu, G.; Tan, Z.; Zhang, D.; Wang, Y.; Li, J.; Ricardez-Sandoval, L. Machine learning in solid heterogeneous catalysis: Recent developments, challenges and perspectives. *Chem. Eng. Sci.* **2022**, *248*, 117224.
4. Melián-Cabrera, I. Catalytic materials: Concepts to understand the pathway to implementation. *Ind. Eng. Chem. Res.* **2021**, *60*, 18545–18559.
5. Pan, Y.; Shen, X.; Yao, L.; Bentalib, A.; Peng, Z. Active sites in heterogeneous catalytic reaction on metal and metal oxide: Theory and Practice. *Catalysts* **2018**, *8*, 478. [CrossRef]
6. Kumar, A.; Belwal, M.; Maurya, R.R.; Mohan, V.; Vishwanathan, V. Heterogeneous catalytic reduction of anthropogenic pollutant, 4-nitrophenol by Au/AC nanocatalysts. *Mater. Sci. Energy Technol.* **2019**, *2*, 526–531. [CrossRef]
7. García-Serna, J.; Piñero-Hernanz, R.; Durán-Martín, D. Inspirational perspectives and principles on the use of catalysts to create sustainability. *Catal. Today* **2022**, *387*, 237–243. [CrossRef]
8. Sulman, E.M.; Matveeva, V.G.; Bronstein, L.M. Design of biocatalysts for efficient catalytic processes. *Curr. Opin. Chem. Eng.* **2019**, *26*, 1–8. [CrossRef]
9. Li, Z.; Hong, R.; Zhang, Z.; Wang, H.; Wu, X.; Wu, Z. Single-atom catalysts in environmental engineering: Progress, outlook and challenges. *Molecules* **2023**, *28*, 3865.
10. SKhan, A.; Khan, S.B.; Asiri, A.M. Layered double hydroxide of Cd-Al/C for the mineralization and de-coloration of dyes in solar and visible light exposure. *Sci. Rep.* **2016**, *6*, 35107.
11. Rahman, M.M.; Khan, S.B.; Asiri, A.M.; Alamry, K.A.; Khan, A.A.P.; Khan, A.; Rub, M.A.; Azum, N. Acetone sensor based on solvothermally prepared ZnO doped with Co_3O_4 nanorods. *Microchim. Acta* **2013**, *180*, 675–685.
12. Védrine, J.C. Importance, features and uses of metal oxide catalysts in heterogeneous catalysis. *Chin. J. Catal.* **2019**, *40*, 1627–1636.
13. Védrine, J.C. Heterogeneous catalysis on metal oxides. *Catalysts* **2017**, *7*, 341.
14. Sohni, S.; Norulaini, N.A.N.; Hashim, R.; Khan, S.B.; Fadhullah, W.; Omar, A.K.M. Physicochemical characterization of Malaysian crop and agro-industrial biomass residues as renewable energy resources. *Ind. Crops Prod.* **2018**, *111*, 642–650.
15. Sharma, R.K.; Bandichhor, R.; Mishra, V.; Sharma, S.; Yadav, S.; Mehta, S.; Arora, B.; Rana, P.; Dutta, S.; Solanki, K. Advanced metal oxide-based nanocatalysts for the oxidative synthesis of fine chemicals. *Mater. Adv.* **2023**, *4*, 1795–1830.
16. Manjunathan, P.; Marakatti, V.S.; Chandra, P.; Kulal, A.B.; Umbarkar, S.B.; Ravishankar, R.; Shanbhag, G.V. Mesoporous tin oxide: An efficient catalyst with versatile applications in acid and oxidation catalysis. *Catal. Today* **2018**, *309*, 61–76.

17. Bakhsh, E.M.; Akhtar, K.; Fagieh, T.M.; Asiri, A.M.; Khan, S.B. Sodium alginate nanocomposite based efficient system for the removal of organic and inorganic pollutants from wastewater. *Int. J. Biol. Macromol.* **2021**, *191*, 243–254.
18. Bakhsh, E.M.; Akhtar, K.; Fagieh, T.M.; Khan, S.B.; Asiri, A.M. Development of alginate@tin oxide–cobalt oxide nanocomposite based catalyst for the treatment of wastewater. *Int. J. Biol. Macromol.* **2021**, *187*, 386–398.
19. Maurya, A.; Yadav, M. Sphere shaped Mo-doped transition metal oxide as electrocatalyst for oxygen evolution reaction in alkaline medium. *J. Alloys Compd.* **2023**, *956*, 170208.
20. Wang, L.; Zhou, S.; You, M.; Yu, D.; Zhang, C.; Gao, S.; Yu, X.; Zhao, Z. Research progress on metal oxides for the selective catalytic reduction of NOx with ammonia. *Catalysts* **2023**, *13*, 1086.
21. Lavrynenko, O.M.; Zahornyi, M.M.; Vember, V.V.; Pavlenko, O.Y.; Lobunets, T.F.; Kolomys, O.F.; Povnitsa, O.Y.; Artiukh, L.O.; Naumenko, K.S.; Zahorodnia, S.D.; et al. Nanocomposites based on cerium, lanthanum, and titanium oxides doped with silver for biomedical application. *Condens. Matter* **2022**, *7*, 45. [CrossRef]
22. Choudhari, U.; Jagtap, S. Lanthanum doped tin oxide: Synthesis, characterization and application. *Mater. Today Proc.* **2022**, *49*, 3325–3330. [CrossRef]
23. Nasrollahzadeh, M.; Akbari, R.; Sakhaei, S.; Nezafat, Z.; Banazadeh, S.; Orooji, Y.; Hegde, G. Polymer supported copper complexes/nanoparticles for treatment of environmental contaminants. *J. Mol. Liq.* **2021**, *330*, 115668.
24. Sarkar, S.; Guibal, E.; Quignard, F.; SenGupta, A.K. Polymer-supported metals and metal oxide nanoparticles: Synthesis, characterization, and applications. *J. Nanoparticle Res.* **2012**, *14*, 715.
25. Khan, S.A.; Bakhsh, E.M.; Akhtar, K.; Khan, S.B. A template of cellulose acetate polymer-ZnAl/C layered double hydroxide composite fabricated with Ni NPs: Applications in the hydrogenation of nitrophenols and dyes degradation. *Spectrochim. Acta Part A Mol. Biomol. Spectrosc.* **2020**, *241*, 118671. [CrossRef]
26. Das, T.K.; Jesionek, M.; Çelik, Y.; Poater, A. Catalytic polymer nanocomposites for environmental remediation of wastewater. *Sci. Total Environ.* **2023**, *901*, 165772.
27. Benali, F.; Boukoussa, B.; Benkhedouda, N.-E.-H.; Cheddad, A.; Issam, I.; Iqbal, J.; Hachemaoui, M.; Abboud, M.; Mokhtar, A. Catalytic Reduction of Dyes and Antibacterial Activity of AgNPs@Zn@Alginate Composite Aerogel Beads. *Polymers* **2022**, *14*, 4829.
28. Mallakpour, S.; Azadi, E.; Dinari, M. Mesoporous Ca-alginate/melamine-rich covalent organic polymer/cupric oxide-based microgel beads as heterogeneous catalyst for efficient catalytic reduction of hazardous water pollutants. *J. Environ. Chem. Eng.* **2023**, *11*, 109294.
29. Meena, P.L.; Saini, J.K. Synthesis of polymer-metal oxide (PANI/ZnO/MnO_2) ternary nanocomposite for effective removal of water pollutants. *Results Chem.* **2023**, *5*, 100764.
30. Naghash-Hamed, S.; Arsalani, N.; Mousavi, S.B. The catalytic reduction of nitroanilines using synthesized $CuFe_2O_4$ nanoparticles in an aqueous medium. *ChemistryOpen* **2022**, *11*, e202200156. [CrossRef]
31. Nagaraj, K.; Thangamuniyandi, P.; Kamalesu, S.; Dixitkumar, M.; Saini, A.K.; Sharma, S.K.; Naman, J.; Priyanshi, J.; Uthra, C.; Lokhandwala, S.; et al. Silver nanoparticles using Cassia Alata and its catalytic reduction activities of rhodamine6G, methyl orange and methylene blue dyes. *Inorg. Chem. Commun.* **2023**, *155*, 110985. [CrossRef]
32. Naz, M.; Rafiq, A.; Ikram, M.; Haider, A.; Ahmad, S.O.A.; Haider, J.; Naz, S. Elimination of dyes by catalytic reduction in the absence of light: A review. *J. Mater. Sci.* **2021**, *56*, 15572–15608. [CrossRef]
33. Dhoondia, Z.H.; Chakraborty, H. Lactobacillus mediated synthesis of silver oxide nanoparticles. *Nanomater. Nanotechnol.* **2012**, *2*, 1–7. [CrossRef]
34. Li, J.; Chen, C.; Li, J.; Li, S.; Dong, C. Synthesis of tin-glycerate and it conversion into SnO_2 spheres for highly sensitive low-ppm-level acetone detection. *J. Mater. Sci. Mater. Electron.* **2020**, *31*, 16539–16547. [CrossRef]
35. Pervez, M.N.; He, W.; Zarra, T.; Naddeo, V.; Zhao, Y. New sustainable approach for the production of Fe_3O_4/graphene oxide-activated persulfate system for dye removal in real wastewater. *Water* **2020**, *12*, 733. [CrossRef]
36. Heck, K.N.; Wang, Y.; Wu, G.; Wang, F.; Tsai, A.-L.; Adamson, D.T.; Wong, M.S. Effectiveness of metal oxide catalysts for the degradation of 1,4-dioxane. *RSC Adv.* **2019**, *9*, 27042–27049. [CrossRef]
37. Hou, J.; Si, L.; Shi, Z.; Miao, C.; Zhao, Y.; Ji, X.; Hou, Q.; Ai, S. Effective adsorption and catalytic reduction of nitrophenols by amino-rich Cu(I)–I coordination polymer. *Chemosphere* **2023**, *311*, 136903. [CrossRef]
38. Umamaheswari, C.; Lakshmanan, A.; Nagarajan, N.S. Green synthesis, characterization and catalytic degradation studies of gold nanoparticles against congo red and methyl orange. *J. Photochem. Photobiol. B Biol.* **2018**, *178*, 33–39. [CrossRef]
39. Narasaiah, B.P.; Mandal, B.K. Remediation of azo-dyes based toxicity by agro-waste cotton boll peels mediated palladium nanoparticles. *J. Saudi Chem. Soc.* **2020**, *24*, 267–281. [CrossRef]
40. Sherin, L.; Sohail, A.; Amjad, U.-E.-S.; Mustafa, M.; Jabeen, R.; Ul-Hamid, A. Facile green synthesis of silver nanoparticles using Terminalia bellerica kernel extract for catalytic reduction of anthropogenic water pollutants. *Colloid Interface Sci. Commun.* **2020**, *37*, 100276. [CrossRef]
41. Ali, H.S.H.M.; Khan, S.A. Stabilization of various zero-valent metal nanoparticles on a superabsorbent polymer for the removal of dyes, nitrophenol, and pathogenic bacteria. *ACS Omega* **2020**, *5*, 7379–7391. [CrossRef] [PubMed]
42. Sun, H.; Abdeta, A.B.; Kuo, D.-H.; Wu, Q.; Guo, Y.; Zelekew, O.A.; Yuan, Z.; Lin, J.; Chen, X. Activated carbon supported CuSnOS catalyst with an efficient catalytic reduction of pollutants under dark condition. *J. Mol. Liq.* **2021**, *334*, 116079. [CrossRef]

43. Fagieh, T.M.; Bakhsh, E.M.; Khan, S.B.; Akhtar, K.; Asiri, A.M. Alginate/banana waste beads supported metal nanoparticles for efficient water remediation. *Polymers* **2021**, *13*, 4054. [CrossRef] [PubMed]
44. Naseem, K.; Ali, F.; Tahir, M.H.; Afaq, M.; Yasir, H.M.; Ahmed, K.; Aljuwayid, A.M.; Habila, M.A. Investigation of catalytic potential of sodium dodecyl sulfate stabilized silver nanoparticles for the degradation of methyl orange dye. *J. Mol. Struct.* **2022**, *1262*, 132996. [CrossRef]
45. Jones, C.W. On the stability and recyclability of supported metal–ligand complex catalysts: Myths, misconceptions and critical research needs. *Top. Catal.* **2010**, *53*, 942–952. [CrossRef]
46. Shende, V.S.; Saptal, V.B.; Bhanage, B.M. Recent advances utilized in the recycling of homogeneous catalysis. *Chem. Rec.* **2019**, *19*, 2022–2043. [CrossRef] [PubMed]
47. Miceli, M.; Frontera, P.; Macario, A.; Malara, A. Recovery/reuse of heterogeneous supported spent catalysts. *Catalysts* **2021**, *11*, 591. [CrossRef]

Disclaimer/Publisher's Note: The statements, opinions and data contained in all publications are solely those of the individual author(s) and contributor(s) and not of MDPI and/or the editor(s). MDPI and/or the editor(s) disclaim responsibility for any injury to people or property resulting from any ideas, methods, instructions or products referred to in the content.